Article

Mechanical Response Analysis of Asphalt Pavement Structure with Embedded Sensor

Pengcheng Wang [1], Guoqiang Zhong [2], Xue Xin [3,*], Fei Xiao [1], Ming Liang [3,*], Chao Wang [2], Yuepeng Jiao [3], Yanli Zhu [3], Shang Liu [2] and Hao Wang [4]

1   Shandong High-Speed Infrastructure Construction Co., Ltd., Jinan 250014, China
2   Shandong Provincial Communications Planning and Design Institute Group Co., Ltd., Jinan 250101, China
3   School of Qilu Transportation, Shandong University, Jinan 250002, China
4   Shandong Hi-Speed Jiwei Expressway Co., Ltd., Jinan 250200, China
*   Correspondence: xinxue@mail.sdu.edu.cn (X.X.); ming.liang@sdu.edu.cn (M.L.);
     Tel.: +86-1866-162-8291 (M.L.)

Abstract: Long-term and real-time monitoring of asphalt pavement can be carried out by using embedded sensors to perceive and predict structural damage during pavement operation period, so as to avoid sustained development of damage. However, the influence of embedded sensors on the mechanical properties of asphalt pavement structure and the structural optimization of sensing elements needs to be further studied. Based on the finite element numerical simulation method, static load model and three-point bending test mode were conducted with three "pavement-sensor" coupling model without sensor, with embedded I-shape sensor, with embedded corrugated-shape sensor. Three simulated conditions were studied comparatively of the sensing element embedding effect on the mechanical response of asphalt pavement structure. Results show that the sensing elements embedded with the two structures have a certain influence on the stress and strain field of asphalt concrete. Within the range of 60–100 mm the asphalt mixture is in a state of tension; the stress values increase with depth and show a maximum tensile stress state at the bottom of the beam. In the compression zone, the strain of the I-shape sensing element embedded is closer to that of the strain without the sensing element embedded. Along the axis of the two sensing elements, the axial strain of the I-shape sensing element is smoother and uniform, which ensures the deformation coordination in the road state. The optimal length L of the sensing element is 14 cm, the diameter φ of the sensor is 10 mm, and the I-beam length GL is 10 cm.

Keywords: embedded; sensing elements; asphalt pavement; mechanical response

1. Introduction

In recent years, to improve the performance of pavement and extend the service life of pavements, researchers have carried out a lot of studies on the structural mechanics, environmental and traffic monitoring for the structural health monitoring (SHM) of pavements [1–3]. However, traditional external inspection methods cannot obtain mechanical information inside of the pavement structure directly and effectively [4,5]. In order to accurately obtain and assess the damage state and the health performance in the pavement structure, sensors need to be embedded in the pavement structure in order to directly obtain mechanical information such as stress–strain of the pavement [6–8]. The long-term and real-time monitoring of embedded sensing elements and the mechanical–structural response relationships can be used to perceive and predict the structural damage that may be incurred during the operation of the pavement so as to avoid the continuous development of damage to the whole pavement structure [9–11].

To monitor the strain conditions of the pavement structure and pavement materials under actual loading, sensors and sensing devices are very important. Several special peculiarities are necessary for pavement sensors to deal with the harsh condition of pavement,

such as high-temperature resistance, compaction resistance and corrosion resistance, etc. Literature reported the sensors using for pavement structure monitoring, including fiber Bragg grating sensor (FBG) [12], strain gauge sensor [13], temperature sensor [14], pressure sensor [15], humidity sensor and so on.

As an embedded element, the sensor should be deformation coincident with the pavement, which means when the pavement deforms under the traffic load or long period fatigue, the embedded sensor should follow synchronous deformation to obtain the value of the mechanical response. Otherwise, when the modulus of the sensor is rather higher than the pavement, the deformation value of sensor will be lower than the pavement or even there is no deformation; when the modulus of sensor is rather lower than the pavement, the deformation value of sensor will be higher than the pavement. Some researchers [16,17] have focused the importance of deformation coincident between the embedded sensor and matrix. In Zhen Liu et al.'s study [18], the encapsulating material with an elastic modulus of 40 GPa for the FBG sensor and a metallic tube with an elastic modulus of 40 GPa for R sensor were established. One study about the effect of the modulus ratio of the FBG sensor to that of the asphalt mixture on the stability of the regression model suggested that the stability worsens as the modulus ratio increases at the same temperature. Zejiao Dong et al. [19] constructed a certain amount of 4-point bending beams filled with random aggregates and asphalt mortar and embedded with the FBG sensor utilizing the FEM. The simulation results illustrated the diverse effects of the different geometries and moduli of embedded sensors on the stress and strain states of the asphalt mixture. However, in these studies, the modulus of sensor is much higher than the asphalt beam according to the encapsulating material which should be improved with the deformation coincident.

The authors' team have carried out a series of related studies in the previous period [20,21]. The strain sensor based on the polymer sensing materials have been developed and verified with the high accuracy and shown the viability for the SHM of asphalt pavement under severe construction and complex operating environments [11,22]. How does the embedding of the sensor element affect structural mechanics of the asphalt pavement, and which kind of sensor element structure can reduce the impact on the pavement structure to a minimum while ensuring the effects of monitoring? To solve these problems, this paper will use ABAQUS software to conduct the statically step-by-step loading method to investigate the impact of embedded sensing elements on the structure of the asphalt pavement and the mechanical changes of the sensing elements themselves by constructing with two different models of sensing elements and asphalt concrete beams. Furthermore, the structural optimization analysis of the sensing element was also carried out.

2. Experimental Design or Methodology

2.1. Modelling Dimensions and Meshing

The simulation parameters were optimized by two steps. The first step is: three simulated conditions (without sensor, with embedded I-shape sensor, with embedded corrugated-shape sensor) were studied comparatively of the sensing element embedding effect on the mechanical response of asphalt pavement structure. After the analysis conclusion of the preferable I-shaped sensor, the paper continues to analyze the structural optimization design of the I-shaped sensing element, in order to compare and study the influence of the sensing element structure on the asphalt mixture matrix, mainly including sensing element length L, sensing element diameter φ, and I-shaped length GL.

Three simulation conditions were built according to the asphalt concrete three-point bending test. Condition 1 was a model of asphalt concrete without sensing element embedded, condition 2 was a model of asphalt concrete with an I-shaped sensing element embedded, condition 3 was a model of asphalt concrete with a corrugated-shape sensing element embedded, in which the sensing element was placed at the bottom centre of the asphalt concrete. The dimension of the asphalt concrete beam has a length of L = 300 mm, width of W = 100 mm, and height of H = 100 mm. The I-beam-shaped sensing element is endowed with the diameter of φ = 10 mm, length of L = 140 mm and the aluminium I-beam

size of 70 mm × 20 mm × 5 mm. The corrugated-shape sensing element is endowed with the diameter of φ = 10 mm, outer diameter of φ = 16 mm, length of L = 140 mm and evenly distributed with 7 bumps with the bump breadth of 5 mm. The asphalt concrete beams and sensor elements are solid homogeneous bodies with C3D8R units (8-node hexahedral linear reduced integration units). The approximate mesh size for the asphalt concrete beam is 5 mm × 5 mm × 5 mm with a total of 24,000 meshes, and the approximate mesh size for the two shaped sensing elements is 1 mm with a total of approximately 26,000 meshes. The model diagrams of the asphalt concrete, I-beam sensing element and corrugated-shape sensing element are shown in Figure 1.
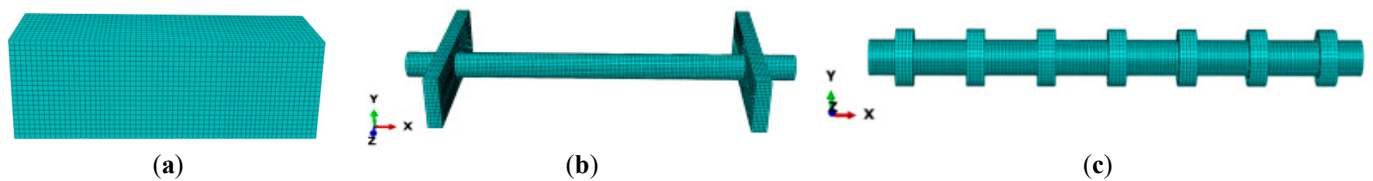

(a) (b) (c)

Figure 1. Component modeling and meshing, (**a**) asphalt concrete, (**b**) I-shaped sensor, (**c**) corrugated-shape sensor.

2.2. Material Parameters

2.2.1. Material Parameters of Asphalt Concrete [23,24]

In this paper, asphalt concrete is assumed to be an isotropic material with Young's modulus of asphalt concrete as 1500 MPa, Poisson's ratio of 0.3, power law multiplier of 6.536×10^{-11}, equivalent force order of 0.937 and time order of -0.592 in creep parameters.

2.2.2. Embedded Sensing Element

Based on the self-developed mechanically sensitive sensor element [25], an isotropic homogeneous elastomer with density of 1500 kg/m^3, modulus of elasticity of 1400 MPa and Poisson's ratio of 0.3 is assumed. The I-beam aluminium alloy is also assumed to be an isotropic homogeneous elastomer with the density of 800 kg/m^3, modulus of elasticity of 72,000 MPa and Poisson's ratio of 0.3 [26–29].

2.3. Boundary Conditions and Load Application

The boundary conditions of the asphalt concrete were imposed according to a three-point bending test. In the model, the asphalt beam was at a free state for the surrounding four sides and fixed constraint at the 30 mm from the edge in the bottom. During the loading, the vertical downward displacement constraint at the top surface were conducted with a statically step-by-step loading mode of loading rate of 0.1 mm/min. The loading target displacement is 1 mm with a total time of 600 s and fixed incremental steps of 12 s.

The stress S11 and strain E11 at the same displacement constraint were obtained along the transverse direction of the asphalt concrete. Six feature points were chosen at 20, 40, 60, 80, 90, and 100 mm from the top of the asphalt concrete in the centre of the asphalt concrete profile, as shown in Figure 2.
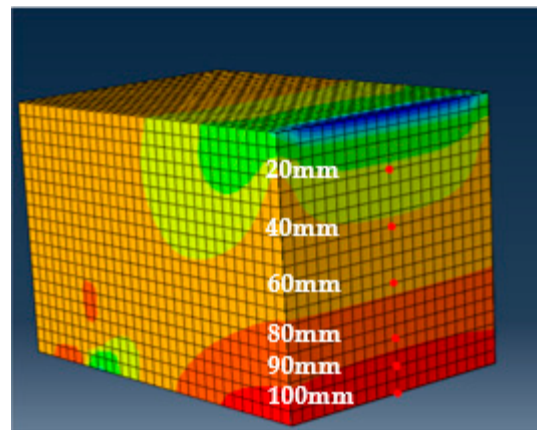
Figure 2. The position of the point in the model.

3. Results and Discussion

3.1. Effect of Embedded Sensing Element on Stress–Strain Field

The schematic diagram of horizontal tensile stress S11, horizontal tensile strain E11 for the exterior of asphalt mixture beam and the central section of the asphalt mixture beam without embedded sensor elements and with embedded sensor elements (I-shaped and corrugated-shape sensor) after the static step-by-step loading simulation are shown in Figure 3.
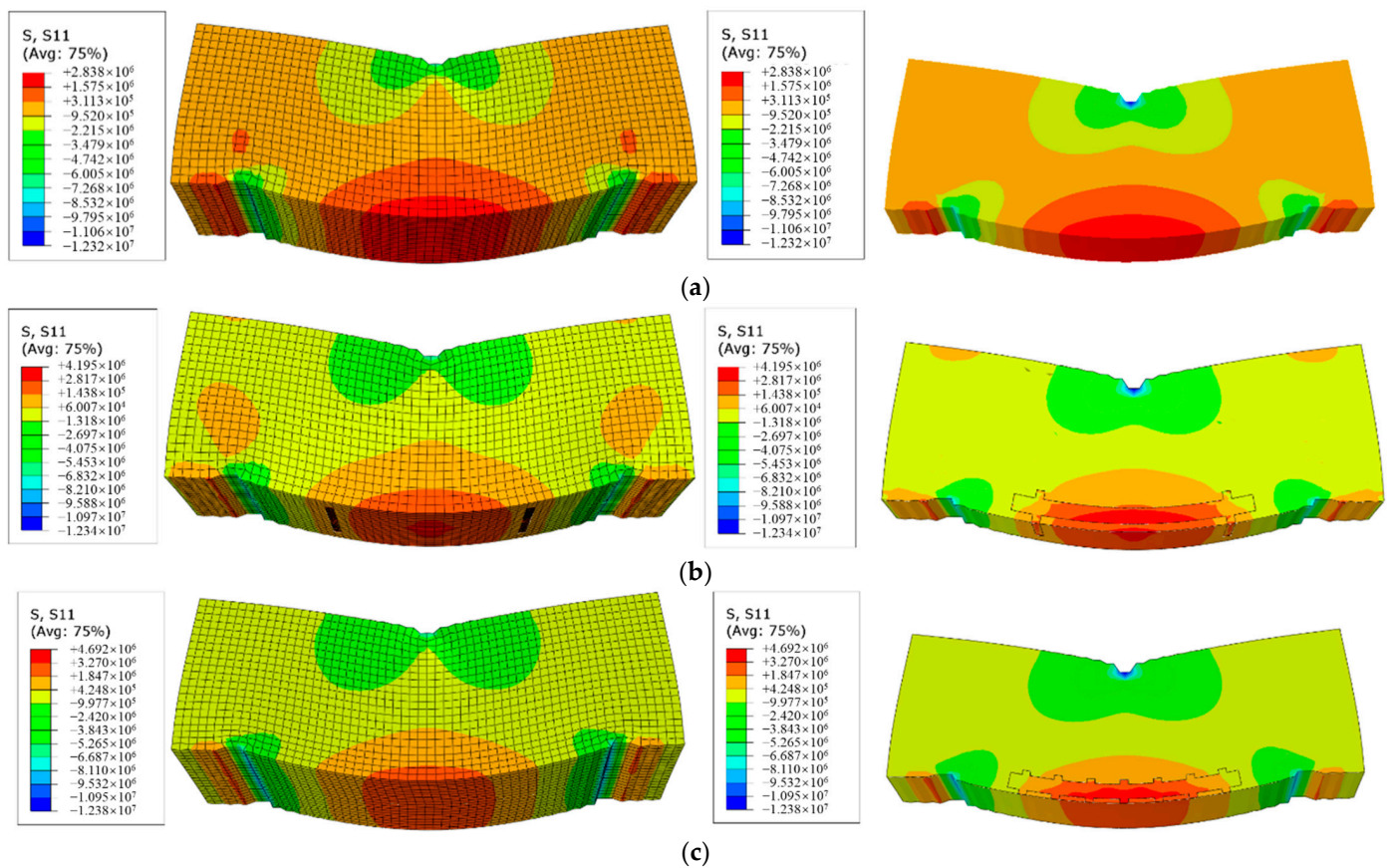

Figure 3. *Cont.*
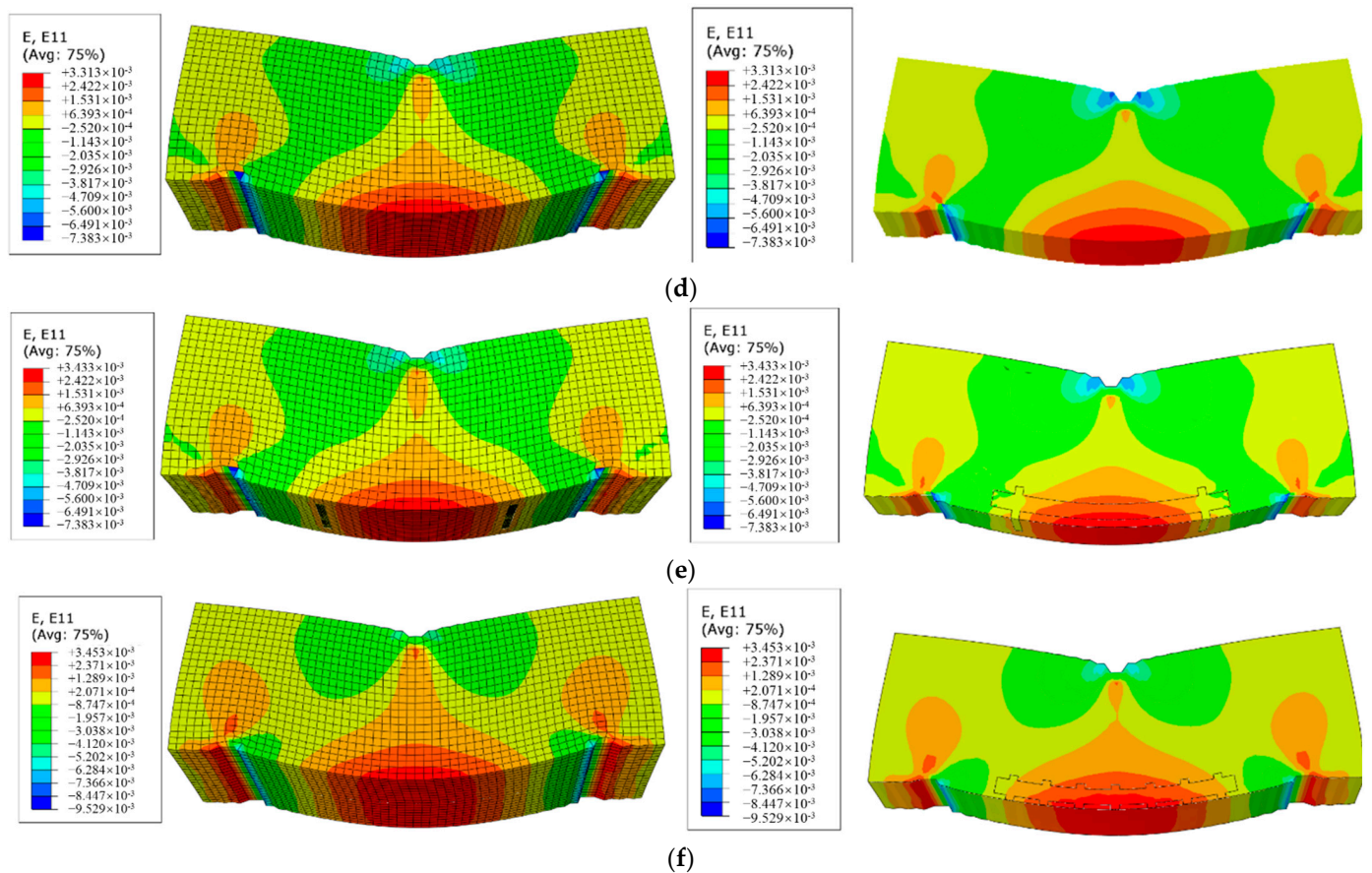
Figure 3. S11 and E11 of asphalt beam under static progressive loading condition, (**a**) S11 without embedded sensors, (**b**) S11 with I-shaped sensor, (**c**) S11 with corrugated-shape sensor, (**d**) E11 without embedded sensors, (**e**) E11 with I-shaped sensor and (**f**) E11 with corrugated-shape sensor.

It can be seen from the figure that the asphalt beams under three conditions show different degrees of loading stresses and strains. The maximum tensile stresses and maximum tensile strains of the asphalt mixture beams with embedded sensors are greater than that in the un-embedded condition, especially for the stress response. The sensor was located at the bottom of the asphalt mixture beam, which just at the location of the maximum tensile stress and maximum tensile strain [30,31].

To describe the tensile stresses and tensile strains at different locations within the asphalt mixture beam and explore the effect of the embedding of sensor elements on the stresses and strains within the structure of the mixture beam more clearly, the variation of S11 and E11 for the selected feature points with vertical loading displacement, are shown in Figure 4.

It can be seen from Figure 4 that in the static step-by-step loading mode, the stress and strain of the asphalt mixture at different locations increase gradually with the increasement of the applied displacement. Within the range of 0–40 mm, the asphalt mixture beam is in a compressed state with negative stress rates. Around the middle of the asphalt mixture beam, the tensile stresses tend towards zero showing the state of neither tensile nor compressive. Within the range of 60–100 mm, the asphalt mixture is in a state of tension, the stress values increase with depth and show a maximum tensile stress state at the bottom of the beam, which is in accordance with the stress conditions during the operation of the asphalt pavement. By comparing Figure 4a–d, the embedment of the sensor element did not have a significant effect on the tensile stresses inside the asphalt mix beams [22].
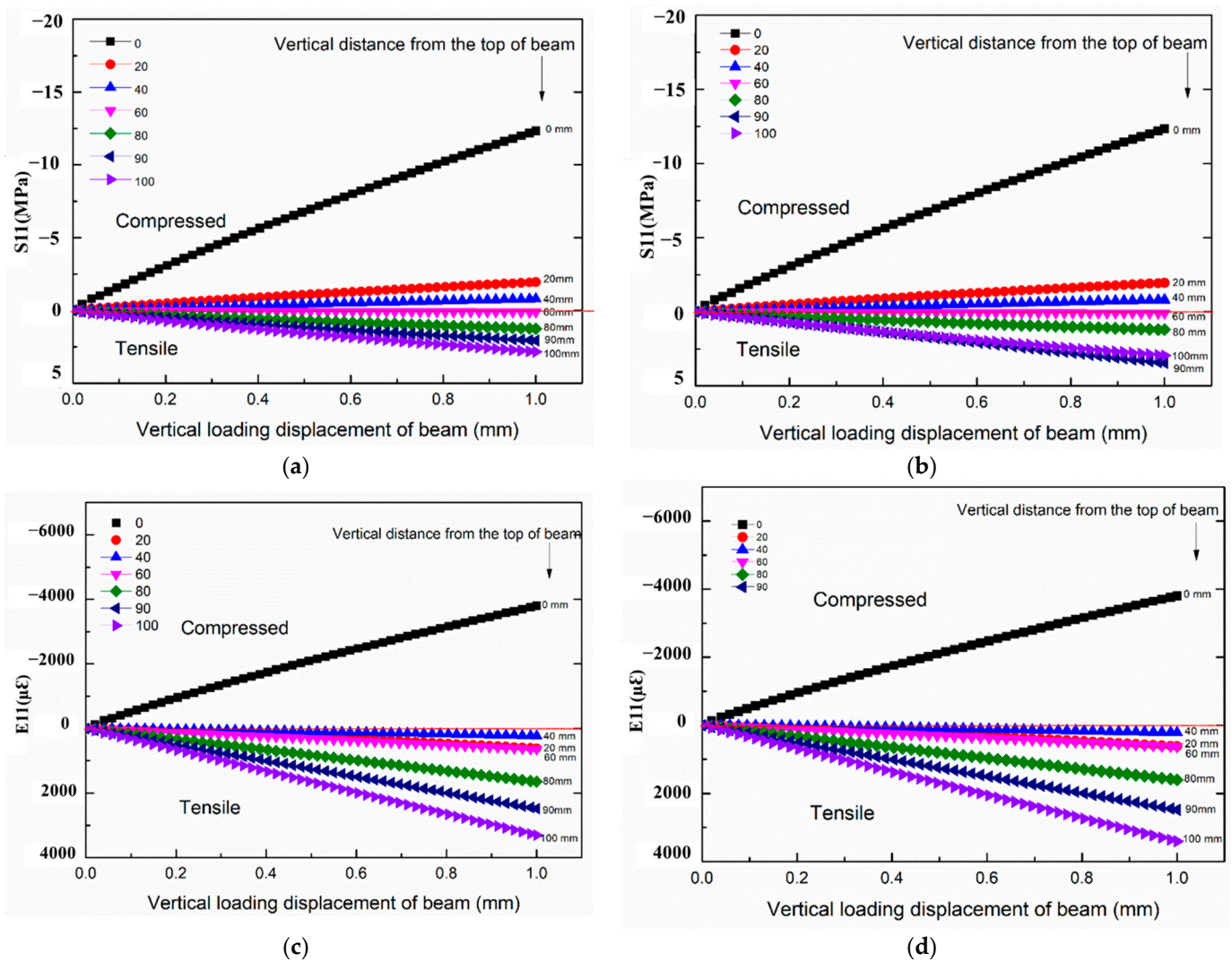
Figure 4. Change of S11 and E11 with the vertical loading displacement, (**a**) S11 of beam without sensor, (**b**) S11 of beam with I-shaped sensor, (**c**) E11 of beam without sensor, (**d**) E11 of beam with I-shaped sensor.

In order to quantitatively compare the effects of the two sensors embedded in different structures on the stress and strain fields in the internal region of the asphalt mixture trabecular, the changes in S11 and E11 with the vertical distance from the top of the trabecular are shown in Figure 5.

It can be seen from Figure 5 that the embedded sensors with two different structures have no great influence on the stress and strain of the asphalt mixture except for the embedded sensing element area. However, compared with the stress and strain curves in Figure 5, the tensile stresses of working condition 2 (embedded I-shape sensor) are much closer to those of working condition 1 (without sensor) than those of working condition 3 (embedded corrugated-shape sensor), indicating that the stress fields of embedded I-shaped sensing element are closer to those of un-embedded sensing element. As for the strain at the embedded area, the differences among the three conditions are almost negligible. Figure 6 shows the tensile strain curves at 90 mm from the top of asphalt mixture (the center of sensor element) under three couple models. It can be seen from the diagram that with the increase in the applied displacement, the tensile strain changes are almost the same under three conditions.
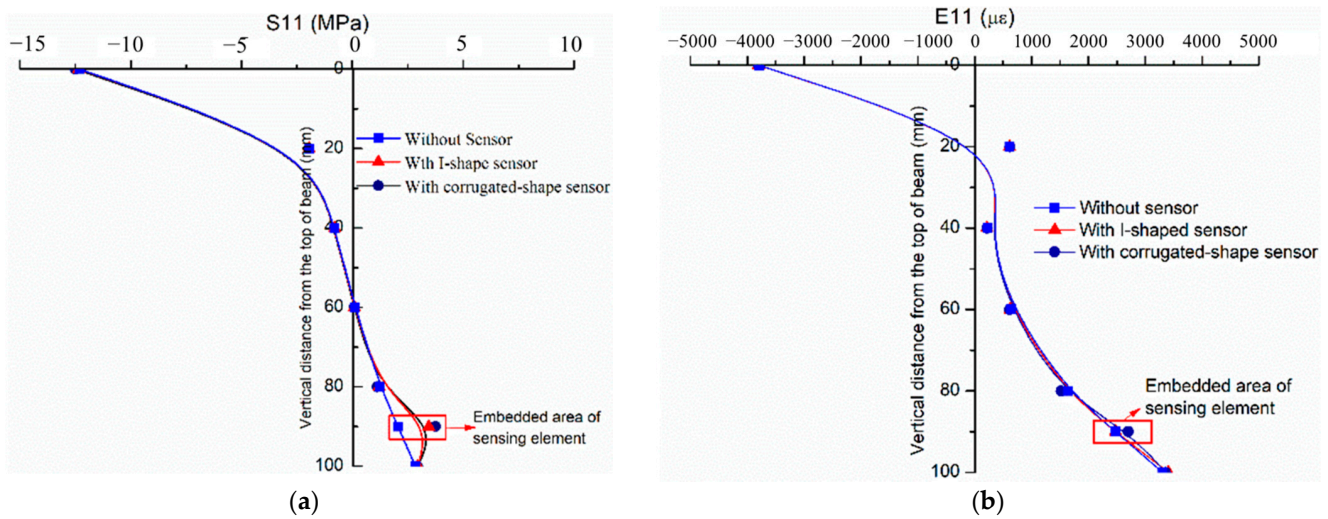
Figure 5. Change in S11 and E11 with the vertical distance from the top of beam, (**a**) S11, (**b**) E11.
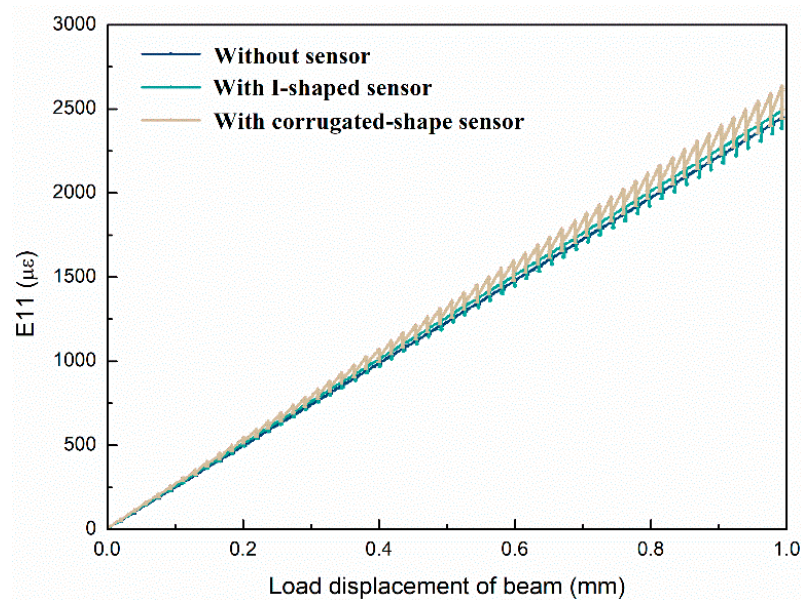

Figure 6. E11 comparison at 90 cm under the three coupling models.

The tensile strain without sensing element of asphalt mixture increases linearly, while the one with sensing element increases in a fluctuating form. Moreover, the tensile strain of the embedded I-shaped sensor is closer to that of the without sensor than that of the embedded corrugated-shape sensor, indicating that the embedded I-shaped sensor has less influence on the asphalt mixture. By comparing, the influence of two embedded sensors with different shapes on the structure of asphalt mixture trabecular is relatively small, but the tensile stress and strain are closer to the asphalt mixture when the I-shaped sensor is embedded. In addition, sensors usually work in different asphalt layers with different gradations and structures, the shape and material of the I-shaped sensor can better ensure the effectiveness, stability and cooperative deformability with the asphalt mixture. Under the actual stress state of the pavement, the pavement structure information obtained by the sensor can better reflect the actual situation of the asphalt pavement [31].

3.2. Horizontal Tensile Strain E11 along the Central Axis of the Sensing Element

To study the stress state of the internal structure of the sensor, the points on the central axis of the sensing element are taken, respectively, as shown in Figure 7.
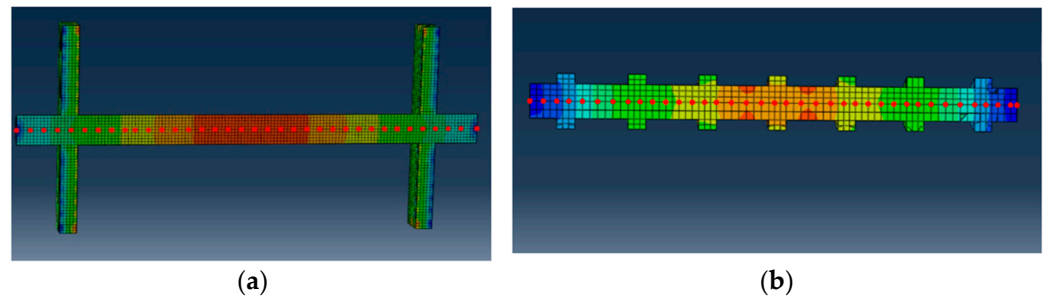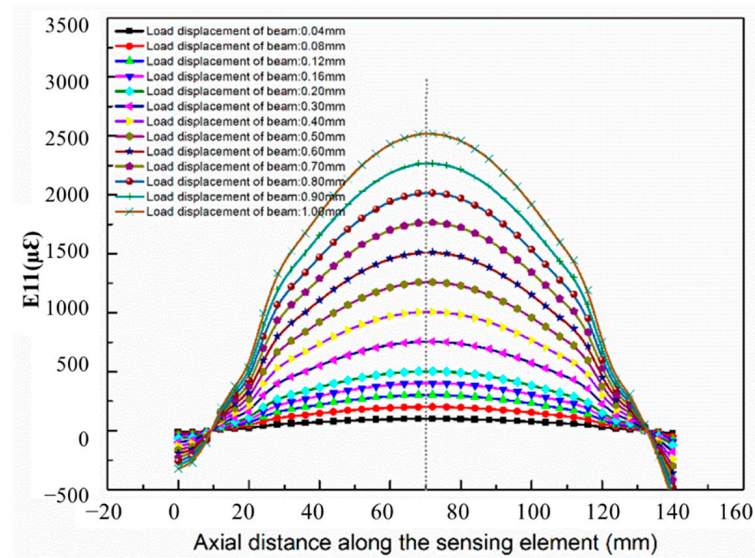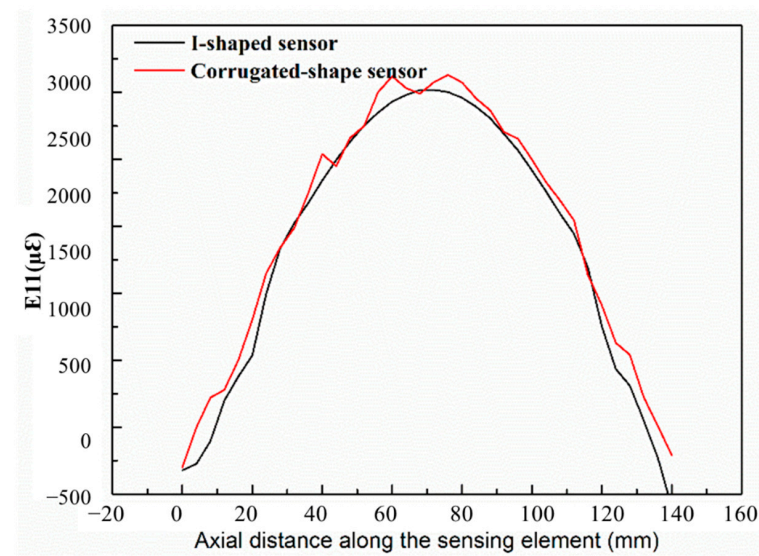
(**a**)   (**b**)

Figure 7. Axial point of sensing element, (**a**) points of the I-shaped sensor, (**b**) points of the corrugated-shape sensor.

Figure 8a shows the variation of the horizontal tensile strain at each point on the axis of the sensing element.

(**a**)

(**b**)

Figure 8. The change of horizontal tension strain E11 along the axial distance of the sensor, (**a**) I-shaped sensing element, (**b**) comparison of two structural sensors.

The horizontal tensile strain E11 on the sensing element gradually increases as the load displacement at the top of the trabecular increases step by step. The horizontal tensile strain shows a trend of increase and then decrease along the axial distance of the sensing element at the central axis of the sensing element, and the maximum horizontal tensile strain occurs at the axial center of the sensing element. This variation law of tensile strain is consistent with the asphalt mixture trabecular itself, which fully verifies the deformation compatibility of the sensing element and the asphalt mixture matrix.

By comparing the embedded sensing elements with two different structures, the largest strain of the sensing element is at the center of the sensing element, and there is a transverse compression area at the end. However, the transition of strain curve is smoother when the I-shaped sensor is embedded. When the corrugated-shape sensing element is embedded, there are many inflection points in the strain curve. If the corrugated-shape sensing element is embedded in the road, it may lead to the internal deformation of the sensing element that cannot be completely consistent when it is subjected to the road load, thereby affecting the monitoring accuracy.

3.3. Structure Optimization Design of Embedded Sensor

The research on the influence of two kinds of sensing elements on the internal mechanical characteristics of asphalt mixture and the deformation characteristics of the sensing element structure show that the I-shaped sensing element is superior to the corrugated-shaped sensing element. Therefore, this paper will continue to analyze the structural optimization design of I-shaped sensing element, in order to compare and study the influence of the sensing element structure on asphalt mixture matrix, mainly including sensing element length L, sensing element diameter φ, and I-shaped length GL. Combined with the actual engineering application, the working condition parameters are selected as shown in Table 1, and the structural optimization modeling examples and simulation results are shown in Figures 9 and 10, respectively.

Table 1. I-shape sensing element structure optimization design parameters.

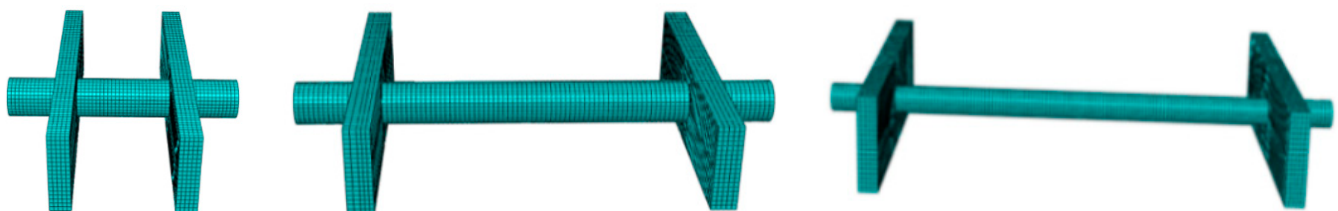| Structure Optimization	Parameters			
Length of sensor L/cm	6	10	14	18
Diameter of sensor φ/mm	6	10	14	/
Length of I-beam GL/cm	3	7	10	/

Figure 9. Schematic diagram of structural optimization modeling for the I-sensor.

Shear stress describes the internal stress concentration of asphalt mixture caused by the embedding of sensing elements. Stress concentration will lead to the slip of the interface between asphalt pavement and sensing element, resulting in loose and falling off of asphalt pavement structure, and then causing pavement diseases. It can be seen from Figure 10a that, with the increase in the sensor length L, the maximum horizontal tensile stress S11 gradually decreases, and the maximum shear stress S12 gradually increases.
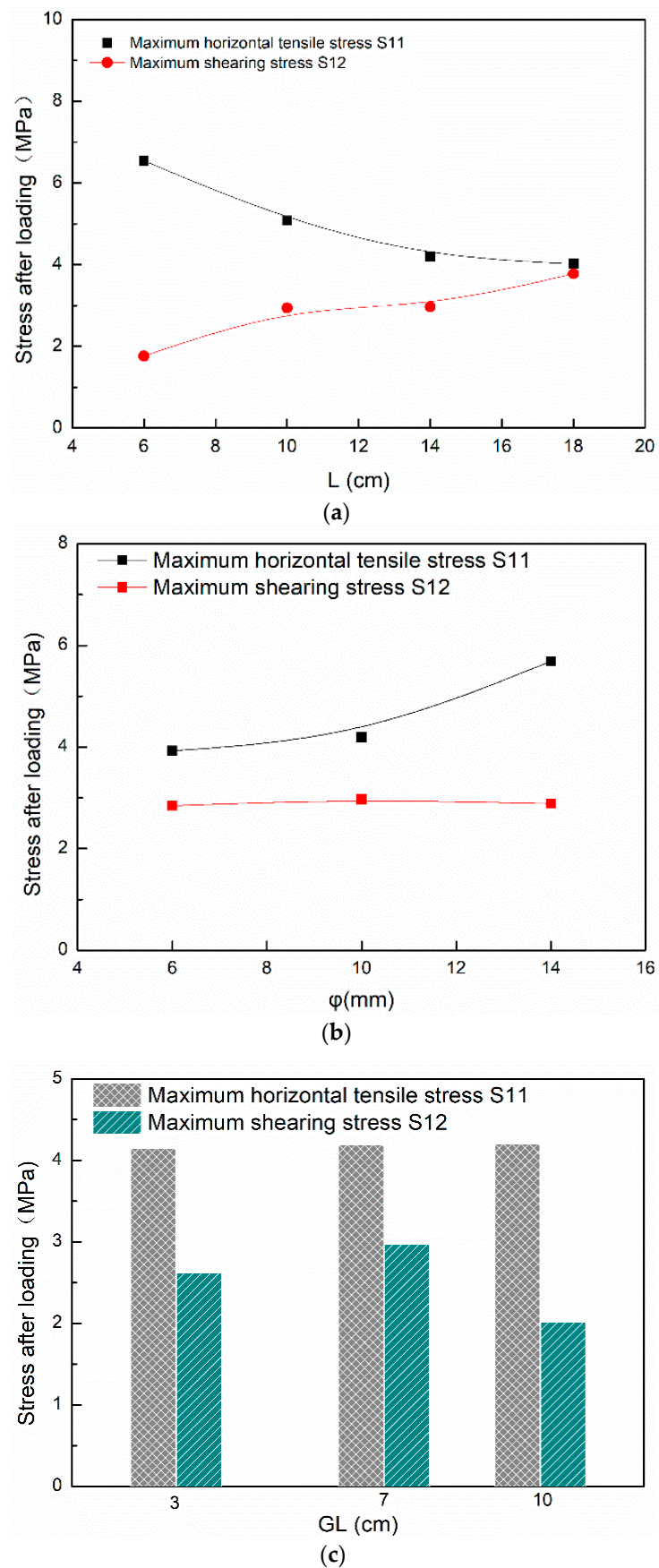
Figure 10. Optimization of I-sensor structure, (**a**) sensing element length optimization, (**b**) sensing element diameter optimization, (**c**) I-beam length optimization.

However, both S11 and S12 have inflection points when L = 14 cm. When L increases from 14 to 16 cm, the decrease in S11 slows down, and the increase in S12 grows significantly. In a comprehensive comparison, the optimal length L of the sensing element is 14 cm. Similarly, the optimal diameter φ of the sensor is 10 mm, and the optimal I-beam length GL is 10 cm.

4. Conclusions

1. In this work, static load model and three-point bending test mode were conducted with three "pavement sensor" coupling model of without sensor, embedded I-shape sensor, embedded corrugated-shape sensor based on the finite element numerical simulation. Three simulated conditions were studied comparatively of the sensors embedding effect on the mechanical response of the asphalt pavement structure.
2. The sensors embedded with the two structures have little influence on the stress and strain field of asphalt concrete. Within the range of 60–100 mm, the asphalt mixture is in a state of tension; the stress values increase with depth and show a maximum tensile stress state at the bottom of the beam. In the compression zone, the strain information is consistent for both the sensors modeled but more consistent for the I-shaped sensor with the actual pavement information.
3. Along the axis of the two sensing elements, the axial strain of the I-shaped sensor is smoother and uniform, which ensures the deformation coordination in the road state.
4. The stress concentration phenomenon occurred on the surface of both sensing elements, but considering that, under actual action, the sensing element embedded in the pavement is subjected to repeated vehicle loads from the pavement, the use of I-shaped sensors can meet the requirements of both durability and structure working.
5. The optimal length L of the sensing element is 14 cm, diameter φ of the sensor is 10 mm, I-beam length GL is 10 cm.

The encapsulating material with an elastic modulus of the sensor have significant impact on the deformation coincident with the pavement, we should choose the encapsulating material with modulus of as close as the asphalt concrete as well as the proper geometries of sensors. Even though the study of embedded sensors has obtained some development, the authors will continue to carry out some simulation work mainly focusing on two areas in the future. One is the asphalt beam with the embedded sensor at the loading stage of dynamic cyclic loading. The other one is to establish the hierarchical model of road structure and insert the sensor elements to simulate the response.

Author Contributions: P.W., X.X. and M.L.: Data curation, Writing—original draft, Writing—review and editing. G.Z. and F.X.: Data curation. C.W. and Y.J.: Investigation. Y.Z.: Investigation. S.L.: Methodology. H.W.: Funding acquisition. All authors have read and agreed to the published version of the manuscript.

Institutional Review Board Statement: Not applicable.

Informed Consent Statement: Not applicable.

Conflicts of Interest: The authors declared that they have no conflict of interest to this work. We declare that we do not have any commercial or associative interest that represents a conflict of interest in connection with the work submitted.

References

1. Brownjohn, J.M.W. Structural health monitoring of civil infrastructure. Philosophical Transactions of the Royal Society A: Mathematical. *Phys. Eng. Sci.* **2007**, *365*, 589–622.
2. Meng, L.; Wang, L.; Hou, Y.; Yan, G. A Research on Low Modulus Distributed Fiber Optical Sensor for Pavement Material Strain Monitoring. *Sensors* **2017**, *17*, 2386. [CrossRef] [PubMed]
3. Timm, D.H.; Priest, A.L.; Mcewen, T.V. *Design and Instrumentation of the Structural Pavement Experiment at the NCAT Test Track*; America National Center for Asphalt Technology (US): Auburn, AL, USA, 2004.
4. Barriera, M.; Pouget, S.; Lebental, B.; Van Rompu, J. In Situ Pavement Monitoring: A Review. *Infrastructures* **2020**, *5*, 18. [CrossRef]
5. Sony, S.; Laventure, S.; Sadhu, A. A literature review of next-generation smart sensing technology in structural health monitoring. *Struct. Control Health Monit.* **2019**, *26*, e2321. [CrossRef]
6. Zappino, E.; Carrera, E. Advanced modeling of embedded piezo-electric transducers for the health-monitoring of layered structures. *Int. J. Smart Nano Mater.* **2020**, *11*, 325–342. [CrossRef]
7. Yan, J.; Luo, D.; Li, Y.; Cafiso, A. Influence of Sensing Element on Mechanical Properties of Asphalt Pavement Substrate. *J. Transp. Res.* **2021**, *7*, 115–123.
8. Mustafa, S.; Sekiya, H.; Maeda, I.; Takaba, S.; Hamajima, A. Identification of external load information using distributed optical fiber sensors embedded in an existing road pavement. *Opt. Fiber Technol.* **2021**, *67*, 102705. [CrossRef]
9. Ko, J.M.; Ni, Y.-Q. Technology developments in structural health monitoring of large-scale bridges. *Eng. Struct.* **2005**, *27*, 1715–1725. [CrossRef]
10. Di Graziano, A.; Marchetta, V.; Cafiso, S. Structural health monitoring of asphalt pavements using smart sensor networks: A comprehensive review. *J. Traffic Transp. Eng. Engl. Ed.* **2020**, *7*, 639–651. [CrossRef]
11. Alavi, A.H.; Hasni, H.; Lajnef, N.; Chatti, K. Continuous health monitoring of pavement systems using smart sensing technology. *Constr. Build. Mater.* **2016**, *114*, 719–736. [CrossRef]
12. Liu, H.; Ge, W.; Pan, Q.; Hu, R.; Lv, S.; Huang, T. Characteristics and analysis of dynamic strain response on typical asphalt pavement using Fiber Bragg Grating sensing technology. *Constr. Build. Mater.* **2021**, *310*, 125242. [CrossRef]
13. Bruno, S.; Del Serrone, G.; Di Mascio, P.; Loprencipe, G.; Ricci, E.; Moretti, L. Technical Proposal for Monitoring Thermal and Mechanical Stresses of a Runway Pavement. *Sensors* **2021**, *21*, 6797. [CrossRef] [PubMed]
14. Lu, R.; Jiang, W.; Xiao, J.; Xing, C.; Ruan, C.; Li, Y.; Wu, W. Temperature characteristics of permeable asphalt pavement: Field research. *Constr. Build. Mater.* **2022**, *332*, 127379. [CrossRef]
15. Raskar, D.; Gadkari, R.; Israji, A.; Mahadik, S. Pavement Pressure Sensor Based Battery Charging and Street Lightning System. *Int. Res. J. Innov. Eng. Technol.* **2022**, *6*, 163.
16. Ye, Z.; Cai, Y.; Liu, C.; Lu, K.; Ildefonzo, D.G.; Wang, L. Optimization of Embedded Sensor Packaging Used in Rollpave Pavement Based on Test and Simulation. *Materials* **2022**, *15*, 2283. [CrossRef] [PubMed]
17. Otto, G.G.; Simonin, J.M.; Piau, J.M.; MattarValente, A. Weigh-in-motion (WIM) sensor response model using pavement stress and deflection. *Constr. Build. Mater.* **2017**, *156*, 83–90. [CrossRef]
18. Liu, Z.; Gu, X.; Wu, C.; Ren, H.; Zhou, Z.; Tang, S. Studies on the validity of strain sensors for pavement monitoring: A case study for a fiber Bragg grating sensor and resistive sensor. *Constr. Build. Mater.* **2022**, *321*, 126085. [CrossRef]
19. Dong, Z.; Ma, X.; Gong, X.; Oeser, M. Theoretical evaluation of the measurement accuracy of fiber Bragg grating strain sensors within randomly filled asphalt mixtures based on finite element simulation. *Struct. Control Health Monit.* **2018**, *25*, e2057. [CrossRef]
20. Xin, X.; Qiu, Z.; Luan, X.; Ding, X.; Liang, M.; Yao, Z.; Li, Y. Novel Conductive Polymer Composites for Asphalt Pavement Structure in Situ Strain Monitoring: Influence of CB/CNT and GNP/CNT Nano/Micro Hybrid Fillers on Strain Sensing Behavior. *IEEE Sens. J.* **2022**, *22*, 3945–3956. [CrossRef]
21. Su, L.; Luan, X.; Qiu, Z.; Liang, M.; Rong, Y.; Xin, X.; Yao, Z.; Ma, C. Sensing Performance and Optimizing Encapsulation Materials of a Coordinated Epoxy-Encapsulated Sensor for Strain Monitoring of Asphalt Pavement Layered Structures. *IEEE Sens. J.* **2022**, *22*, 9811–9823. [CrossRef]
22. Tian, G.; Dong, Z.; Hu, Q. Analysis of cooperative deformation between fiber grating sensor and asphalt mixture. *J. Harbin Inst. Technol.* **2009**, *41*, 73–76.
23. Xin, X.; Liang, M.; Yao, Z.; Su, L.; Zhang, J.; Li, P.; Sun, C.; Jiang, H. Self-sensing behavior and mechanical properties of carbon nanotubes/epoxy resin composite for asphalt pavement strain monitoring. *Constr. Build. Mater.* **2020**, *257*, 119404. [CrossRef]
24. Xin, X.; Rong, Y.; Su, L.; Yao, Z. Dynamic Mechanical and Chemorheology Analysis for the Blended Epoxy System with Polyurethane Modified Resin. *J. Renew. Mater.* **2022**, *10*, 1081. [CrossRef]
25. Xin, X.; Luan, X.; Su, L.; Ma, C.; Liang, M.; Ding, X.; Yao, Z. The Innovative Self-Sensing Strain Sensor for Asphalt Pavement Structure: Substitutability and Synergy Effects of Graphene Platelets with Carbon Nanotubes in Epoxy Composites. *Front. Mater.* **2022**, *9*, 824364. [CrossRef]
26. Awed, A.M.; Tarbay, E.W.; El-Badawy, S.M.; Azam, A.M. Performance characteristics of asphalt mixtures with industrial waste/by-product materials as mineral fillers under static and cyclic loading. *Road Mater. Pavement Des.* **2022**, *23*, 335–357. [CrossRef]
27. Varma, S.; Kutay, M.E. Viscoelastic Nonlinear Multilayered Model for Asphalt Pavements. *J. Eng. Mech.* **2016**, *142*, 04016044. [CrossRef]

28. Li, Q.; Wang, L.; Li, Z. Finite element analysis of asphalt mixture rutting based on dynamic modulus. *Shanxi Archit.* **2019**, *45*, 154–156.

29. Mishra, M.; Lourenço, P.B.; Ramana, G.V. Structural health monitoring of civil engineering structures by using the internet of things: A review. *J. Build. Eng.* **2022**, *48*, 103954. [CrossRef]

30. Liu, W.; Wang, H.; Zhou, Z.; Xing, X.; Cao, D.; Jiang, Z. Optical fiber-based sensors with flexible encapsulation for pavement behavior monitoring. *Struct. Control Health Monit.* **2015**, *22*, 301–313. [CrossRef]

31. Yao, X. Development and Application of Monitoring data Analysis System for Asphalt Pavement Structure Information. Ph.D. Thesis, Harbin Institute of Technology, Harbin, China, 2018; pp. 5–16.